

Photometric detection of internal gravity waves in upper main-sequence stars

IV. Comparable stochastic low-frequency variability in SMC, LMC, and Galactic massive stars

Dominic M. Bowman^{1,2}, Pieterjan Van Daele^{1,2}, Mathias Michielsen², and Timothy Van Reeth²

¹ School of Mathematics, Statistics and Physics, Newcastle University, Newcastle upon Tyne, NE1 7RU, UK
e-mail: dominic.bowman@newcastle.ac.uk

² Institute of Astronomy, KU Leuven, Celestijnenlaan 200D, B-3001 Leuven, Belgium

Received 8 July 2024; accepted 21 October 2024

ABSTRACT

Context. Massive main-sequence stars have convective cores and radiative envelopes, but can also have sub-surface convection zones caused by partial ionisation zones. However, the convective properties of such regions strongly depend on opacity and therefore a star's metallicity. Non-rotating 1D evolution models of main-sequence stars between $7 \leq M \leq 40 M_{\odot}$ and the metallicity of the Small Magellanic Cloud (SMC) galaxy suggest tenuous (if any) sub-surface convection zones when using the Rayleigh number as a criterion for convection owing to their substantially lower metallicity compared to Galactic massive stars.

Aims. We test whether massive stars of different metallicities both inside and outside of asteroseismically calibrated stability windows for sub-surface convection exhibit different properties in stochastic low-frequency (SLF) variability. Thus, we aim to constrain the metallicity dependence of the physical mechanism responsible for SLF variability commonly found in light curves of massive stars.

Methods. We extracted customised light curves from the ongoing NASA Transiting Exoplanet Survey Satellite (TESS) mission for a sample of massive stars using an effective point spread function (ePSF) method, and compared their morphologies in terms of characteristic frequency, ν_{char} , and amplitude using a Gaussian process (GP) regression methodology.

Results. We demonstrate that the properties of SLF variability observed in time series photometry of massive stars are generally consistent across the metallicity range from the Milky Way down to the SMC galaxy, for stars both inside and outside of the sub-surface stability windows based on the Rayleigh number as a criterion for convection.

Conclusions. We conclude that non-rotating 1D stellar structure models of sub-surface convection cannot alone be used to explain the mechanism giving rise to SLF variability in light curves of massive stars. Additionally, the similar properties of SLF variability across a wide range of metallicity values, which follow the same trends in mass and age in the Hertzsprung–Russell (HR) diagram at both high and low metallicity, support a transition in the dominant mechanism causing SLF variability from younger to more evolved stars. Specifically, core-excited internal gravity waves (IGWs) are favoured for younger stars lacking sub-surface convection zones, especially at low metallicity, and sub-surface convection zones are favoured for more evolved massive stars.

Key words. stars: early-type – stars: fundamental parameters – stars: massive – stars: rotation – stars: oscillations

1. Introduction

Our ability to ascertain precise and accurate constraints on the physical processes within massive stars, such as chemical mixing and angular momentum transport, has been revolutionised by studying stellar variability and applying forward asteroseismic modelling (see Bowman 2020 for a review). Identifying coherent self-excited pulsation modes allow one to perform linear asteroseismology by quantitatively comparing observed pulsation mode frequencies to their theoretical counterparts calculated from a grid of stellar structure models (Aerts et al. 2010; Aerts 2021). Coherent pulsations are generally grouped into pressure (p) and gravity (g) modes based on their restoring forces that respectively probe the envelope and deep interior of a massive main-sequence star. Such coherent pulsations are excited by a periodic heat-engine mechanism operating within the iron-nickel opacity bump at 200 000 K (Dziembowski & Pamyatnykh 1993; Dziembowski et al. 1993; Miglio et al. 2007; Szewczuk & Daszyńska-Daszkiewicz 2017). Important constraints from for-

ward asteroseismic modelling of coherent pulsations include interior mixing and rotation profiles, magnetic field strength and geometry, and the efficiency of angular momentum transport (Aerts et al. 2003; Dupret et al. 2004; Pamyatnykh et al. 2004; Dziembowski & Pamyatnykh 2008; Briquet et al. 2012; Salmon et al. 2022; Lecoanet et al. 2022; Burssens et al. 2023).

The necessary data for asteroseismic analyses of massive stars are long-duration time series, either photometric or spectroscopic, spanning at least a few months, but ideally several years (Bowman 2023). Given that high-cadence spectroscopic time series are quite expensive when assembled with ground-based telescopes (see e.g. Aerts et al. 2003), asteroseismology using space-mission light curves has largely driven the field during the last two decades. Space missions with an asteroseismic component include CoRoT (Auvergne et al. 2009), BRITE (Weiss et al. 2014, 2021), *Kepler*/K2 (Borucki et al. 2010; Koch et al. 2010; Howell et al. 2014), and the Transiting Exoplanet Survey Satellite (TESS; Ricker et al. 2015), which together have revealed a diversity of variability mechanisms at work in massive stars (see

e.g. Degroote et al. 2009; Bowman et al. 2019b; Burssens et al. 2020; Zwintz et al. 2024).

Recently, a new form of asteroseismic signal called stochastic low-frequency (SLF) variability was discovered in many massive stars (Bowman et al. 2019a,b), and was shown to directly probe a massive star’s mass and age (Bowman et al. 2020; Bowman & Dorn-Wallenstein 2022). This SLF variability is seemingly ubiquitous in Galactic massive stars with light curve data of sufficiently high photometric precision. After an initial detection in three O stars observed by CoRoT (Blomme et al. 2011), the first large-scale analysis of SLF variability among massive stars revealed a common morphology for dwarf stars with spectral types earlier than B9 (Bowman et al. 2019a). The sample was expanded to include hundreds of massive stars across the sky using photometry from the K2 mission in addition to dozens of blue supergiants in the Large Magellanic Cloud (LMC) galaxy for the first time (Bowman et al. 2019b). Later, combining TESS mission light curves and high-resolution spectroscopy, it was shown that a strong correlation exists between the properties of SLF variability and the location of stars in the Hertzsprung–Russell (HR) diagram (Bowman et al. 2020). Recently, a novel method using Gaussian process (GP) regression confirmed this correlation, and revealed a transition from stochastic to quasi-periodic variability exists for massive Galactic stars during the main sequence (Bowman & Dorn-Wallenstein 2022). For stars without coherent heat-engine pulsation modes it is not possible to apply traditional forward asteroseismic modelling, thus SLF variability has motivated the advent of gravity wave asteroseismology (Bowman 2023).

Various theoretical and multi-dimensional hydrodynamical model predictions, which are not mutually exclusive, for explaining SLF variability in massive stars exist within the literature. Plausible mechanisms include internal gravity waves (IGWs) excited stochastically at the boundary of convective cores (Rogers et al. 2013; Rogers 2015; Edelmann et al. 2019; Horst et al. 2020; Varghese et al. 2023; Ratnasingam et al. 2019, 2020, 2023; Vanon et al. 2023; Herwig et al. 2023; Thompson et al. 2024), waves and/or turbulence caused by sub-surface convection zones (Cantiello et al. 2009, 2021; Schultz et al. 2022), and inhomogeneities in the winds of massive stars (Krtićka & Feldmeier 2018; Krtićka & Feldmeier 2021). However, the last of these mechanisms is expected to play a negligible role for late O-type and early B-type main-sequence stars because of their optically thin and weak winds, especially at low metallicity. The explanation of SLF variability is hotly debated in the literature. Some hydrodynamical simulations suggest that IGWs excited by core convection reach the surface with smaller amplitudes than the observed amplitudes for SLF variability, which suggests that it arises from another convective region (Lecoanet et al. 2019, 2021; Le Saux et al. 2023; Anders et al. 2023). However, owing to the numerical challenges, hydrodynamical studies have generally not yet been performed using 3D spherical geometry with comparable rotation rates to observed stars. Moreover, some studies have shown that higher angular degree IGWs (i.e. $\ell \gtrsim 30$) make a significant contribution to mixing in the deep interiors of massive stars, and can potentially explain the shape of SLF variability at a star’s surface (Herwig et al. 2023; Thompson et al. 2024). This means that predictions from damping of high- ℓ in simulations can be quite sensitive to the numerical set-up, which in turn can make a quantitative comparison of different simulations to observations fairly challenging.

Recently, Jermyn et al. (2022) demonstrated using non-rotating 1D stellar structure models that late O and early B main-sequence stars at low metallicity may not have sub-surface con-

vection zones when the Rayleigh number is considered as a necessary criterion for convection. This calls into question whether sub-surface convection zones in the envelopes of massive stars at low metallicity are really regions with convection as the dominant transport mechanism and whether they can excite IGWs. Regardless, IGWs generated by turbulent core convection are not mutually exclusive with IGWs generated by sub-surface convection zones. Observations suggest a possible transition between IGWs excited by core convection being dominant at the zero-age main sequence (ZAMS) to IGWs excited by sub-surface convection being dominant at the terminal-age main sequence (TAMS) in the HR diagram for Galactic massive stars (Bowman & Dorn-Wallenstein 2022). This transition remains unexplored outside of Galactic massive stars.

For this work, paper IV in the current series, we used new TESS observations and advanced light curve extraction techniques applied to massive stars in the Small Magellanic Cloud (SMC) galaxy and compared them to stars in the LMC and the Milky Way. Our specific goal was to test whether a common morphology exists for SLF variability across a wide range of metallicities, keeping in mind the possible absence of sub-surface convection zones in low-metallicity massive stars (Jermyn et al. 2022). In Sect. 2 we describe the calculation of 1D stellar structure and evolution models to define sub-surface convection stability windows, and in Sect. 3 we describe our target star selection criteria and TESS light curve extraction methodology. In Sect. 4 we present and discuss our analysis of the light curves and SLF variability, and we conclude in Sect. 5.

2. Sub-surface convection stability windows

2.1. Rayleigh number as a criterion for convection

Recently, Jermyn et al. (2022) investigated the properties of sub-surface convection zones using the 1D stellar evolution code MESA (Paxton et al. 2011, 2013, 2015, 2018, 2019; Jermyn et al. 2023). They investigated whether the envelopes of massive stars satisfy the Rayleigh number, Ra , as a criterion for convection, which is defined as

$$Ra \equiv \frac{g(\nabla_{\text{rad}} - \nabla_{\text{ad}})\delta r^3}{\nu\alpha} \left(\frac{\delta r}{h}\right) \left(\frac{4-3\beta}{\beta}\right), \quad (1)$$

where ∇_{rad} and ∇_{ad} are the radiative and adiabatic temperature gradients, g is the gravitational acceleration, δr is the thickness of the Ledoux-unstable layer, ν is the kinematic viscosity, α is the thermal diffusivity, h is the pressure scale height, and β is the radiation parameter (cf. Appendices B and D of Jermyn et al. 2022 and references therein). The Rayleigh number indicates the importance of buoyancy when compared to diffusive processes, such that when $Ra < Ra_{\text{crit}}$ buoyancy is insufficient to overcome diffusive processes and convection cannot occur.

Jermyn et al. (2022) used the Rayleigh number to test whether sub-surface convection zones, associated with partial ionisation zones of metals (e.g. iron), helium, and hydrogen, are present for stars spanning $7 \leq M \leq 40 M_{\odot}$ and from the onset of core-hydrogen burning (i.e. ZAMS) until core-hydrogen exhaustion (i.e. TAMS). Using Eq. (1) as a condition for convective instability, Jermyn et al. (2022) demonstrated that massive stars with Galactic metallicity always have a sub-surface convection zone within their envelopes during the main sequence. However, for lower metallicities, such as stars in the SMC and LMC galaxies, there exists a parameter space in the HR diagram for which only the convective core satisfies the Rayleigh number, such that

there are no sub-surface convection zones. Jermyn et al. (2022) defined these parameter spaces as ‘stability windows’ in the HR diagram in which the partial ionisation zones of metals, hydrogen, and helium are not convection zones. Therefore, given the significant differences in the convective properties of stellar envelopes between metal-rich and metal-poor stars, the properties of SLF variability observed in the light curves of such stars may be different if these zones are acting as the physical mechanism responsible for SLF variability.

2.2. Asteroseismic MESA models

In this work, we expand upon the previous study of Jermyn et al. (2022) by including convective boundary mixing (CBM) and envelope mixing calibrated by asteroseismology. This is important because interior mixing has a large impact on the width of the main sequence in the HR diagram and on the maximum radius and age of a massive star at the TAMS. A growing number of asteroseismic studies have demonstrated the importance of a non-negligible amount of CBM in massive main-sequence stars (Dupret et al. 2004; Pamyatnykh et al. 2004; Dziembowski & Pamyatnykh 2008; Briquet et al. 2011; Burssens et al. 2023). In particular, a non-zero amount of CBM facilitates unprocessed hydrogen from the envelope to be transported into the nuclear-burning core, thus extending the main-sequence lifetime by at least 25% and displacing the TAMS to cooler effective temperatures in the HR diagram (Bowman 2020).

We calculated a grid of non-rotating evolutionary tracks using MESA (v15140) for stars with masses $7 \leq M \leq 40 M_{\odot}$, a metal mass fraction consistent with the SMC (i.e. $Z = 0.002 \approx 0.2 Z_{\odot}$), and ages that span from the ZAMS to the TAMS. We included a fixed amount of envelope mixing (i.e. $\log(D_{\text{env}}) = 3.0$) and a range in CBM using the diffusive exponential mixing prescription (i.e. $0.0 \leq f_{\text{ov}} \leq 0.3$) as inferred from detailed forward asteroseismic modelling of pulsating stars within and proximate to this parameter space (e.g. Michielsen et al. 2021; Pedersen et al. 2021; Burssens et al. 2023). For completeness, we also calculated a second grid of MESA models with the same range of parameters except that the metal mass fraction was consistent with the LMC (i.e. $Z = 0.006 \approx 0.5 Z_{\odot}$).

Our sub-surface convection zone stability windows that encompass the full range of minimum to maximum values of CBM inferred from asteroseismology are shown as the combined yellow and blue regions in Fig. 1. We chose to be conservative in the definition of the stability windows, and specifically show models that satisfy $Ra < 0.001 Ra_{\text{crit}}$ (cf. Eq. (1)), thus demonstrating that the Rayleigh number criterion for the lack of convection is robustly satisfied. The transition just beyond the edge of the stability windows from $Ra \sim Ra_{\text{crit}}$ to $Ra < 0.001 Ra_{\text{crit}}$ is extremely sharp in the HR diagram. The stability windows cover a larger parameter space in the HR diagram compared to those of Jermyn et al. (2022) because of the non-zero amount of CBM. We show the evolutionary tracks with the minimum and maximum values of CBM as solid and dashed lines, respectively, which displaces the TAMS to cooler temperatures and higher luminosities because of the extended main-sequence lifetime being at least 25% longer in massive stars that include non-zero CBM. As expected, the size of the stability window for SMC metallicity is much larger than for LMC metallicity (Jermyn et al. 2022).

3. TESS light curves of SMC and LMC massive stars

TESS is an all-sky time series photometric survey mission observing individual sectors of the sky for up to 27 d (Ricker et al.

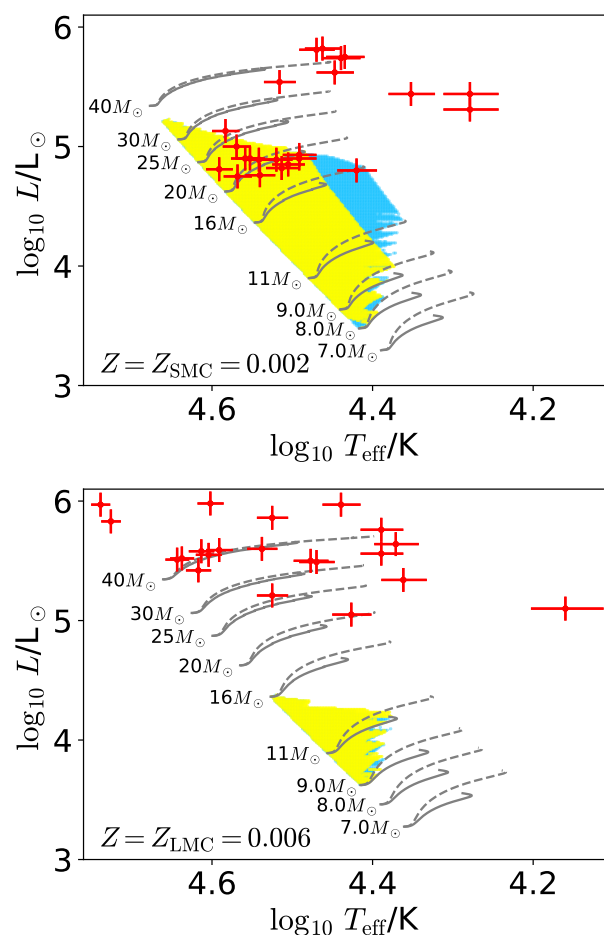


Fig. 1. Hertzsprung–Russell (HR) diagram for SMC stars (i.e. $Z = 0.002$; top panel) and LMC stars (i.e. $Z = 0.006$; bottom panel) with evolutionary tracks of different masses between the ZAMS and the TAMS. The sub-surface convection zone stability windows as defined by the region for which $Ra < 0.001 Ra_{\text{crit}}$ (cf. Eq. (1)) are shown in yellow for models with minimum mixing and blue for the additional models with maximum values of mixing. Evolutionary tracks with minimum and maximum mixing are shown as solid and dashed lines, respectively. The location of the sub-sample of stars with reliable TESS light curves, all of which have significant SLF variability, are shown as red points.

2015). Its primary science case is to identify candidate exoplanet transits orbiting bright Galactic stars. TESS provides its entire field of view spanning four cameras as full-frame images (FFIs) at a cadence of 200 s starting from its second extended mission (Jenkins et al. 2016). Previous FFI cadences were 30 min and 10 min in the nominal mission and first extended mission, respectively. Bias subtraction and flat fielding were performed before delivery of FFIs to the Mikulski Archive of Space Telescopes (MAST¹).

3.1. SMC and LMC sample selection

As our goal is to investigate the occurrence and properties of SLF variability of massive stars at low metallicity, we require a bona fide sample of massive stars in the SMC and LMC galaxies to place in the HR diagram. Massive stars, including dwarfs, giants, and supergiants of spectral types earlier than about B9 in the LMC have been studied spectroscopically thanks to Very

¹ <https://archive.stsci.edu/missions-and-data/tess>

Table 1. Parameters of SMC massive stars proximate to and within the sub-surface convection zone stability window studied in this work.

Simbad name	TIC ID	Gaia DR3	T_{eff} (K)	$\log_{10}(L/L_{\odot})$	ν_{char} (d^{-1})	PSD_{max} ($\text{mmag}^2/\text{d}^{-1}$)	PSD_{min} ($\text{mmag}^2/\text{d}^{-1}$)
AzV 16	180617038	4685854571724688768	27200	5.75	$0.33^{+0.08}_{-0.09}$	2.43×10^{-3}	3.29×10^{-7}
AzV 18	180617057	4688950933906863488	19000	5.44	$0.35^{+0.17}_{-0.18}$	1.06×10^{-3}	2.57×10^{-7}
AzV 83	181043369	4688966125248119808	32800	5.54	$0.88^{+0.13}_{-0.12}$	7.69×10^{-4}	4.74×10^{-6}
CI* NGC 346 MPG 12	181880133	4689016221756858624	31000	4.93	$0.96^{+0.20}_{-0.17}$	4.26×10^{-4}	1.10×10^{-5}
AzV 202	181887485	4689019898248677888	26300	4.80	$2.04^{+1.97}_{-0.95}$	1.68×10^{-5}	4.25×10^{-6}
CI* NGC 346 ELS 46	182294016	4690504582501410432	39000	4.81	$2.10^{+9.16}_{-1.74}$	2.87×10^{-3}	1.13×10^{-4}
CI* NGC 346 ELS 25	182294030	4690504994818102016	36200	4.90	$0.73^{+0.15}_{-0.13}$	3.02×10^{-3}	3.64×10^{-5}
AzV 267	182294155	4690507022042458624	35700	4.90	$1.47^{+6.93}_{-0.63}$	5.30×10^{-4}	3.26×10^{-5}
AzV 264	182294249	4690520387983090432	22500	5.44	$0.40^{+0.08}_{-0.09}$	1.17×10^{-3}	3.59×10^{-7}
AzV 251	182300503	4685990709381204864	33100	4.89	$2.69^{+10.02}_{-1.11}$	9.92×10^{-5}	6.16×10^{-6}
CI* NGC 346 MPG 682	182300967	4689015465842590464	34800	4.89	$0.73^{+3.54}_{-0.66}$	4.71×10^{-3}	2.99×10^{-5}
AzV 372	182729695	4687411518857964032	28000	5.62	$0.48^{+0.09}_{-0.09}$	5.46×10^{-4}	2.50×10^{-7}
AzV 429	182910549	4687532533854919680	38300	5.13	$1.03^{+0.24}_{-0.19}$	1.39×10^{-4}	6.14×10^{-6}
AzV 468	183302393	4687248791131672960	34700	4.76	$7.78^{+16.26}_{-6.98}$	4.66×10^{-5}	1.07×10^{-5}
AzV 479	183306464	4686408759936714752	29000	5.82	$1.05^{+0.18}_{-0.20}$	2.36×10^{-5}	1.46×10^{-7}
AzV 472	183306676	4687241472507227520	19000	5.31	$0.49^{+0.08}_{-0.09}$	2.54×10^{-4}	1.87×10^{-7}
AzV 488	183492668	4686413437158238208	27500	5.74	$0.56^{+0.10}_{-0.10}$	1.75×10^{-4}	7.58×10^{-8}
[M2002] SMC 81469	183979145	4686450580031889536	31000	4.90	$1.99^{+0.39}_{-0.30}$	4.21×10^{-5}	2.50×10^{-6}
2dFS 3780	183981879	4686448106130736256	32000	4.85	$1.39^{+0.36}_{-0.28}$	1.58×10^{-5}	2.39×10^{-6}
2dFS 163	267429694	4688838203919272832	32600	4.82	$1.48^{+0.30}_{-0.25}$	4.00×10^{-4}	1.21×10^{-5}
2dFS 3954	303910981	4686266721070836608	37000	4.75	$2.95^{+16.79}_{-1.97}$	4.29×10^{-5}	1.12×10^{-5}
AzV 461	402099597	4687470686324401536	37100	5.00	$0.36^{+0.12}_{-0.14}$	5.76×10^{-3}	4.50×10^{-6}
AzV 456	402100664	4687251368112248960	29500	5.81	$0.83^{+0.21}_{-0.24}$	2.95×10^{-5}	2.04×10^{-7}

Notes. Spectroscopic parameters are from Vink et al. (2023) and Hawcroft et al. (2024), and the characteristic frequency, ν_{char} , and its 2σ confidence interval determined using a Gaussian process (GP) regression methodology (Bowman & Dorn-Wallenstein 2022). The maximum and minimum values of the power spectral density (PSD) of the best-fit GP regression model, as proxies for α_0 and C_w , respectively, of the SLF variability are also provided. An average for the typical reported uncertainties are $\sigma(T_{\text{eff}}) = 1500$ K and $\sigma(\log_{10}(L/L_{\odot})) = 0.1$ dex.

Large Telescope (VLT) programmes with European Southern Observatory (ESO) instruments, such as VLT-Flames (PI: Smart) and its successor the VLT-Flames Tarantula Survey (VFTS; PI: Evans), and more recently the ongoing Binarity at Low Metallicity (BLOeM) survey for the SMC (PI: Shenar; Shenar et al. 2024). Breakthroughs in studying LMC massive stars include the metallicity dependence of winds and mass loss (Mokiem et al. 2007), empirical rotation rates (Ramírez-Agudelo et al. 2013), surface-nitrogen abundances and their relation to interior mixing (Hunter et al. 2008), and constraints on binary statistics (Sana et al. 2012).

The *Hubble* Space Telescope (HST) recently completed an unprecedented number of orbits as part of a Director’s Discretionary Time (DDT) project called Ultraviolet Legacy Library of Young Stars as Essential Standards (ULLYSES²; Roman-Duval et al. 2020). The ULLYSES project is targeting over 250 massive stars in the SMC and LMC, with the HST data consisting of high-quality COS and STIS UV spectra. To support these data, an ESO large program, X-Shooting ULLYSES (XShooU³), has assembled medium-resolution optical spectra with the XShooter spectrograph (Vernet et al. 2011). Spectroscopic parameters, in

particular effective temperature and luminosity, are available from the first papers from the XShooU collaboration (Vink et al. 2023; Hawcroft et al. 2024), but are also supplemented by spectroscopic studies by Mokiem et al. (2006) and Bouret et al. (2013).

3.2. TESS light curve extraction

There are two major challenges to overcome to extract reliable TESS light curves of SMC and LMC stars. We note that the TESS mission was not designed for this purpose, and hence specialised software tools are needed and a moderately high failure rate in this work is inevitable. The first challenge is that distant stars beyond the Milky Way are quite faint for the brightness limit of the TESS mission. Second, such stars are usually contaminated since they suffer from high crowding and blending in the relatively large pixels (21 arcsec) of the TESS CCDs. These limitations have the potential to severely limit astrophysical inference based on light curves extracted using standard simple aperture photometry (SAP) techniques, which is common for Galactic massive stars (see e.g. Bowman et al. 2022).

² <https://ullyses.stsci.edu>

³ <https://massivestars.org/xshootu/>

Table 2. Parameters of LMC massive stars proximate to the sub-surface convection zone stability window studied in this work.

Simbad name	TIC ID	Gaia DR3	T_{eff} (K)	$\log_{10}(L/L_{\odot})$	ν_{char} (d^{-1})	PSD_{max} ($\text{mmag}^2/\text{d}^{-1}$)	PSD_{min} ($\text{mmag}^2/\text{d}^{-1}$)
[L72] LH 9–89	30275740	4662154018793644928	26700	5.05	$0.80^{+0.37}_{-0.31}$	9.89×10^{-3}	6.16×10^{-6}
[ELS2006] N11 051	30275973	4662156630134021376	41400	5.42	$2.50^{+1.11}_{-0.65}$	3.67×10^{-5}	1.64×10^{-6}
Sk –66 18	30312045	4662202878335589376	40200	5.55	$2.87^{+1.79}_{-0.82}$	1.55×10^{-5}	5.69×10^{-7}
[ELS2006] N11 046	30313090	4662144501145651328	33500	5.21	$1.17^{+1.10}_{-0.43}$	4.43×10^{-4}	5.24×10^{-6}
Sk –68 41	31105740	4661392533937464448	24500	5.56	$0.42^{+0.05}_{-0.06}$	5.71×10^{-4}	9.05×10^{-8}
Sk –68 52	31181554	4661289630893455488	24500	5.76	$0.32^{+0.06}_{-0.07}$	1.18×10^{-3}	8.90×10^{-8}
Sk –65 22	55758033	4662240708409788928	33500	5.86	$0.67^{+0.09}_{-0.10}$	2.63×10^{-4}	1.29×10^{-7}
W61 28–5	276936126	4657275137819689216	44000	5.51	$0.93^{+0.18}_{-0.15}$	1.61×10^{-4}	4.52×10^{-6}
VFTS 72	277300368	4657698454092124416	54800	5.97	$1.04^{+0.16}_{-0.16}$	4.76×10^{-5}	1.15×10^{-6}
Sk –66 17	277103700	4660278492484698112	29500	5.49	$1.06^{+0.11}_{-0.10}$	9.97×10^{-5}	2.13×10^{-7}
BI 237	277105480	4660109236409051392	53200	5.83	$1.04^{+6.09}_{-0.29}$	9.09×10^{-6}	5.99×10^{-7}
VFTS 244	277300097	4657680552664841856	41050	5.58	$1.87^{+0.48}_{-0.39}$	4.94×10^{-4}	2.43×10^{-5}
VFTS 355	277300563	4657688695923883648	43400	5.52	$1.08^{+0.13}_{-0.11}$	3.99×10^{-5}	2.33×10^{-6}
Sk –68 135	277300709	4657700790554314752	27500	5.97	$0.24^{+0.09}_{-0.12}$	2.99×10^{-3}	6.42×10^{-8}
Sk –71 35	287436747	4651835961162249984	23000	5.34	$0.35^{+0.08}_{-0.10}$	5.85×10^{-3}	4.76×10^{-7}
Sk –66 100	373849172	4660223379469868416	39000	5.59	$2.75^{+4.79}_{-1.03}$	1.60×10^{-5}	3.99×10^{-7}
BI 173	373919576	4658104341338342528	34500	5.60	$2.42^{+4.29}_{-0.95}$	1.34×10^{-5}	3.21×10^{-7}
RMC 109	391746326	4660181151347435008	14450	5.10	$0.27^{+0.08}_{-0.10}$	8.41×10^{-4}	1.47×10^{-7}
Sk –71 41	391887962	4651834994760055040	30000	5.50	$0.77^{+0.09}_{-0.09}$	1.43×10^{-4}	2.55×10^{-7}
Sk –68 140	404768212	4657688313632701568	23500	5.64	$0.48^{+0.09}_{-0.10}$	8.72×10^{-4}	2.78×10^{-7}
Sk –67 166	425083410	4660121743354291328	40000	5.98	$1.39^{+0.11}_{-0.12}$	4.33×10^{-5}	1.33×10^{-7}

Notes. Spectroscopic parameters are from Vink et al. (2023) and Hawcroft et al. (2024), and the characteristic frequency, ν_{char} , and its 2σ confidence interval determined using a Gaussian process (GP) regression methodology (Bowman & Dorn-Wallenstein 2022). The maximum and minimum values of the power spectral density (PSD) of the best-fit GP regression model, as proxies for α_0 and C_w , respectively, of the SLF variability are also provided. An average for the typical reported uncertainties are $\sigma(T_{\text{eff}}) = 1500$ K and $\sigma(\log_{10}(L/L_{\odot})) = 0.1$ dex.

To overcome these challenges, we used the `tg1c` software package⁴, which allows a user to extract light curves of (faint and blended) TESS targets using an effective point spread function (ePSF) fitting methodology (Han & Brandt 2023). This ePSF method has been shown to be effective at disentangling different sources in regions with high crowding because it uses a Bayesian framework with priors for source locations informed by Gaia astrometry (Gaia Collaboration et al. 2016, 2023). We refer to Han & Brandt (2023) for full technical and numerical details of the well-documented and open-source `tg1c` software tool. We performed testing against other PSF-fitting software tools (e.g. `photutils`; Bradley et al. 2022), and concluded that the `tg1c` software provides, on average, a more robust light curve extraction, especially when compared to standard SAP approaches applied to SMC and LMC massive stars (Van Daele 2023).

As a sanity check, we visually inspected all the diagnostic plots provided by the `tg1c` software package and the extracted ePSF light curves for all stars. Unsuccessful cases were easily flagged based on the standard deviation of the extracted ePSF light curve exceeding 50 mmag, which is primarily because such a light curve is dominated by systematics or extremely high Poisson noise levels because it contains very little flux from the stellar target and is dominated by background flux. The typical amplitudes of SLF variability for Galactic massive stars are

well below this (e.g. Bowman et al. 2019b, 2020), meaning that unsuccessful cases are easily flagged automatically. In general, we were guided by previous studies of Galactic massive stars with TESS (e.g. Bowman et al. 2020, 2022) in terms of the typical amplitude and period ranges of coherent pulsations and SLF variability in massive stars. Since SMC and LMC massive stars have (much) larger noise levels in their light curves compared to Galactic stars, because they are (much) fainter, we were unable to probe the faintest stars in the XShootU sample, which correspond to the lowest mass stars (i.e. late-B stars). Unfortunately, the majority of the XShootU sample of massive stars are quite faint and/or too heavily blended to extract reliable light curves even with the ePSF methodology.

To be classified as a successful case, each star had to pass all the quality checks discussed above, but we also checked for consistent signatures of SLF variability in its light curve in at least two consecutive TESS sectors (if available since several SMC stars only have a single TESS sector). Consistent in this context means a star has comparable SLF variability morphology (i.e. the same ν_{char} value within a 2σ confidence interval) in at least two TESS sectors. Successful cases were subsequently detrended using a low-order polynomial to remove any remaining long-period instrumental artefacts, which is necessary and typical for TESS mission data (see Bowman et al. 2020, 2022). From the XShootU sample of SMC and LMC stars, we defined

⁴ https://github.com/TeHanHunter/TESS_Gaia_Light_Curve

a sub-sample of 23 successfully extracted SMC massive stars that are within or proximate to the sub-surface convection zone stability window including asteroseismically calibrated amounts of CBM (cf. Fig. 1). Additionally, we were able to extract reliable light curves for 21 LMC massive stars, but these are all outside of their corresponding sub-surface convection zone stability window. The names and spectroscopic parameters of the sub-samples of SMC and LMC massive stars are provided in Tables 1 and 2, respectively, and the location of these sub-samples in the HR diagram are shown in Fig. 1. We note that the SMC sub-sample includes stars both inside and outside of the sub-surface convection zone stability window, allowing us to investigate differences in the observed SLF variability.

4. SLF variability in SMC and LMC massive stars

Starting from the XShootU sample, we identified a sub-sample of 23 SMC massive stars that satisfy the following criteria: (i) reliable stellar parameters in the literature; (ii) proximate to or within the sub-surface convection zone stability windows that include CBM calibrated by asteroseismology; and (iii) robust ePSF light curves extracted using the `tg1c` software package (Han & Brandt 2023). The locations of the SMC and LMC sub-samples in the HR diagram in relation to our calculated evolution tracks and the corresponding sub-surface convection stability windows are shown in Fig. 1.

We fitted the extracted ePSF light curves using the Gaussian process (GP) regression light curve fitting methodology of Bowman & Dorn-Wallenstein (2022) based on the `celerite2` software package⁵ (Foreman-Mackey et al. 2017, 2019). Similarly to Bowman & Dorn-Wallenstein (2022), who applied this method to Galactic massive stars, we used a damped simple harmonic oscillator (SHO) kernel with a damping timescale, τ_{damp} ; amplitude, σ_A ; and characteristic variability timescale, ρ_{damp} (from which a characteristic frequency, ν_{char} , can be calculated), as free parameters, all with large uniform priors. An additional term for the jitter, C_w , was also included, which is related to the amount of white noise in a light curve and is assigned a Gaussian prior with a width corresponding to standard deviation of the light curve (see Bowman & Dorn-Wallenstein 2022). With best-fit parameters determined by the GP regression method, we then estimated the statistical confidence intervals for all GP regression free parameters using a Hamiltonian Monte Carlo with a no U-turn sampler (NUTS) using the `pymc3` software package⁶ (Salvatier et al. 2016). The resultant ν_{char} values and their 2σ confidence intervals for the sub-samples of SMC and LMC stars are provided in Tables 1 and 2, respectively. This numerical analysis methodology was shown to be more efficient and more robust against systematic uncertainties when analysing SLF variability in Galactic massive stars compared to directly fitting an amplitude spectrum with a Lorentzian-like function (Bowman & Dorn-Wallenstein 2022).

After fitting the light curves for all stars in our SMC and LMC sub-samples, it is immediately clear that the vast majority of the stars exhibit SLF variability similar to their Galactic counterparts (e.g. Bowman et al. 2019a,b, 2020). This is confirmed using model selection and a Bayesian information criterion (BIC) to invalidate a white noise-only model following a similar approach used by Bowman & Dorn-Wallenstein (2022). We recall that the faintest stars in our sample correspond to the lowest mass main-sequence stars in the SMC; we expect these

stars to have the smallest amplitudes in their SLF variability, but also the noisiest light curves. Therefore, we demonstrate for the first time that SLF variability is also common across a wide range of metallicity values, as well as mass and age for stars above $\sim 20 M_{\odot}$. We show the TESS light curves, frequency spectra, and GP regression model for the SMC and LMC sub-samples of stars in Figs. A.1–A.3 and A.4–A.6, respectively.

For comparison, we define a third sub-sample of Galactic massive stars based on the best-fitting GP regression models for 30 massive stars in the Milky Way from Bowman & Dorn-Wallenstein (2022). We show histograms of the important GP regression fitting parameters for all the massive stars across the Milky Way, LMC and SMC sub-samples in Fig. 2. Interestingly, the amplitude of the SLF variability is slightly lower on average for the SMC sub-sample of massive stars compared to the LMC. This is achieved by defining a signal-to-noise ratio (S/N) of SLF variability as the ratio of the maximum and minimum values in the power spectral density (PSD) of the GP regression fit. These serve as useful proxies for α_0 and C_w , respectively (cf. Bowman et al. 2020), and allow a comparison of stars with very different white noise contributions in their light curves. The values of PSD_{max} and PSD_{min} are given in Tables 1 and 2, for the SMC and LMC sub-samples, respectively. For example, the inferred value of the amplitude of the SLF variability in a frequency spectrum in SMC stars can be artificially higher if inferred from directly fitting a frequency spectrum because of the increased contribution of white noise (i.e. C_w), which can be large within the sub-sample of SMC stars. With the caveat of it being a small sample of stars to compare, the histograms in Fig. 2 show similar values for S/N; characteristic frequency, ν_{char} ; damping timescale, τ_{damp} ; and quality factor, Q , across the three metallicity regimes.

We find similar morphologies of SLF variability for stars in the SMC regardless of whether they are located inside or outside of their corresponding stability window. However some stars in both the SMC and LMC sub-samples have noisier detections of SLF variability owing to relatively high levels of Poisson (i.e. white) noise in their light curves. All SLF variability fits are statistically significant according to model selection compared to a white noise-only model using the corresponding BIC values (cf. Bowman & Dorn-Wallenstein 2022). Some noisier detections of SLF variability yield (much) larger relative uncertainties in their inferred ν_{char} values (i.e. of order 100% or more) and/or low S/N values (i.e. < 100) in their SLF variability. We note that such stars remain robust detections of SLF variability, but are not necessarily well-characterised stars in terms of their inferred ν_{char} values owing to having, on average, noisier light curves.

Notwithstanding the caveat of lower mass stars having noisier light curves, on average, we note a trend in that SMC and LMC sub-samples of stars closer to the ZAMS having generally smaller S/N values in their SLF variability compared to those closer to the TAMS, albeit with a large amount of scatter. This agrees with the same trend found by Bowman et al. (2020) in that the amplitude of SLF variability is a function of main-sequence age for Galactic massive stars. This means that the same trend with age is apparent for low-metallicity stars as Galactic massive stars. However, the small sample size, the relatively large errors, and the scatter in this trend mean that we cannot use the amplitude of SLF variability to validate or invalidate different interpretations for the physical mechanism causing SLF variability. On the other hand, this trend does demonstrate that the evolutionary properties of a massive star can be probed from its light curve as shown previously by Bowman et al. (2020).

To further demonstrate the common morphology of SLF variability across all metallicity regimes, the correlations among

⁵ <https://celerite2.readthedocs.io/en/latest/>

⁶ <https://docs.pymc.io/en/v3/index.html>

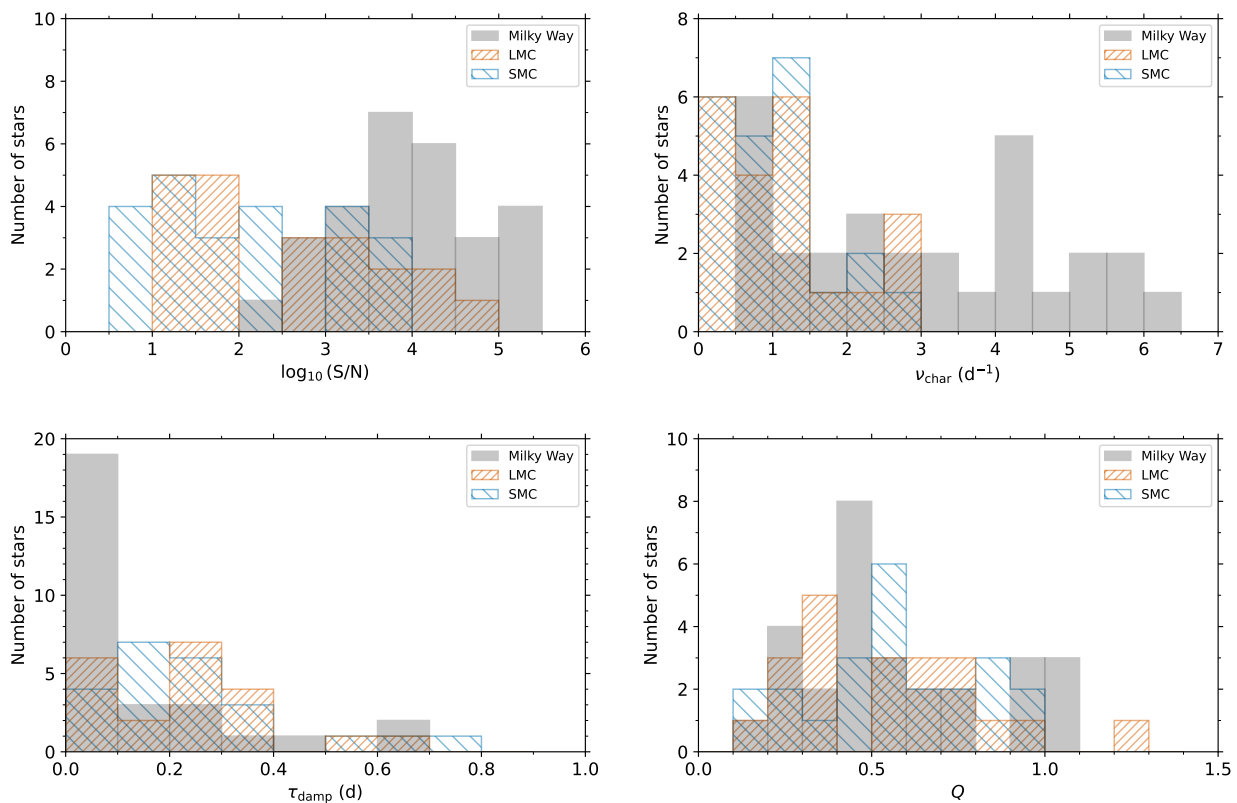


Fig. 2. Histograms of the signal-to-noise ratio (S/N); characteristic frequency, ν_{char} ; damping timescale, τ_{damp} ; and the quality factor, Q , of SLF variability for the Milky Way, LMC, and SMC massive stars.

the S/N; characteristic frequency, ν_{char} ; and damping timescale, τ_{damp} , of the SLF variability for the sub-samples of Galactic, LMC, and SMC massive stars studied in this work are colour-coded by luminosity, and are shown in Fig. 3. For the Milky Way sub-sample stars, we use the spectroscopic effective luminosity with values from Bowman et al. (2020), which is defined as $\mathcal{L} := T_{\text{eff}}^4/g$ (Langer & Kudritzki 2014), due to uncertain values in galactic extinction and reddening and to be consistent with the previous analyses of SLF variability across the HR diagram in this series of papers. The photometric and GP regression fitting parameters are less precise for the LMC and SMC sub-samples, owing to the noisier TESS light curves, but the same trends in Fig. 3 exist in all three sub-samples. As noted by previous studies, the diversity in SLF variability parameters is high, and could be linked to different rotation rates or inclinations of the stars, which give rise to different surface amplitudes of IGWs (see Bowman & Dorn-Wallenstein 2022). However, the similar correlations across all metallicity regimes support a common physical origin for SLF variability that is seemingly insensitive to metallicity. For example, massive low-metallicity stars that are luminous have, on average, lower ν_{char} values and larger SLF variability amplitudes, as previously demonstrated for Galactic massive stars (Bowman et al. 2019b, 2020). It should be noted that the stars with the noisiest light curves, and thus the largest relative uncertainty in their SLF variability morphology, are typically the faintest stars and are at or beyond the nominal operating brightness limit of TESS around $V \gtrsim 13$ mag. It is challenging to draw strong conclusions on the trends of SLF variability in the HR diagram based on the currently available sample because the instrumental and astrophysical biases mean fainter stars have lower masses and also have smaller amplitude SLF variability.

These results lead to two possible conclusions. First, the similar morphology of SLF variability for massive stars in the SMC both inside and outside of the sub-surface convection stability window indicates that SLF variability is unlikely to be exclusively caused by sub-surface convection. This is supported by massive stars having similar morphology in their SLF variability across the metallicity regimes of the Milky Way, LMC, and SMC. However, this assumes that the stability windows (cf. Sect. 2) are based on an accurate implementation of physics in 1D non-rotating structure models, and thus can act as good predictors of observables. A sub-surface stability window does not appear to exist for Milky Way metallicity (Jermyn et al. 2022), and SLF variability is ubiquitous for such stars (Bowman et al. 2019b, 2020). Second, if SLF variability is in fact caused by sub-surface convection, these results imply that 1D structure models do not provide reasonable predictors for observables associated with SLF variability. Both of these conclusions may be correct, which emphasises the need to continue to compare observations to hydrodynamical simulations of stellar interiors with 3D spherical geometry and realistic rotation rates (e.g. Aerts & Rogers 2015; Edelman et al. 2019; Anders et al. 2023).

On the other hand, since the S/N of SLF variability is somewhat lower for SMC stars compared to LMC and Galactic massive stars, it is a reasonable inference that the observed SLF variability arises from both core convection and sub-surface convection. For LMC and Galactic stars, and their somewhat larger SLF variability amplitudes and their more efficient sub-surface convection zones, the observed SLF variability could be comprised of IGWs from both core convection and sub-surface convection. Instead, for SMC stars with their somewhat smaller SLF variability amplitudes and their less efficient (or absent) sub-surface

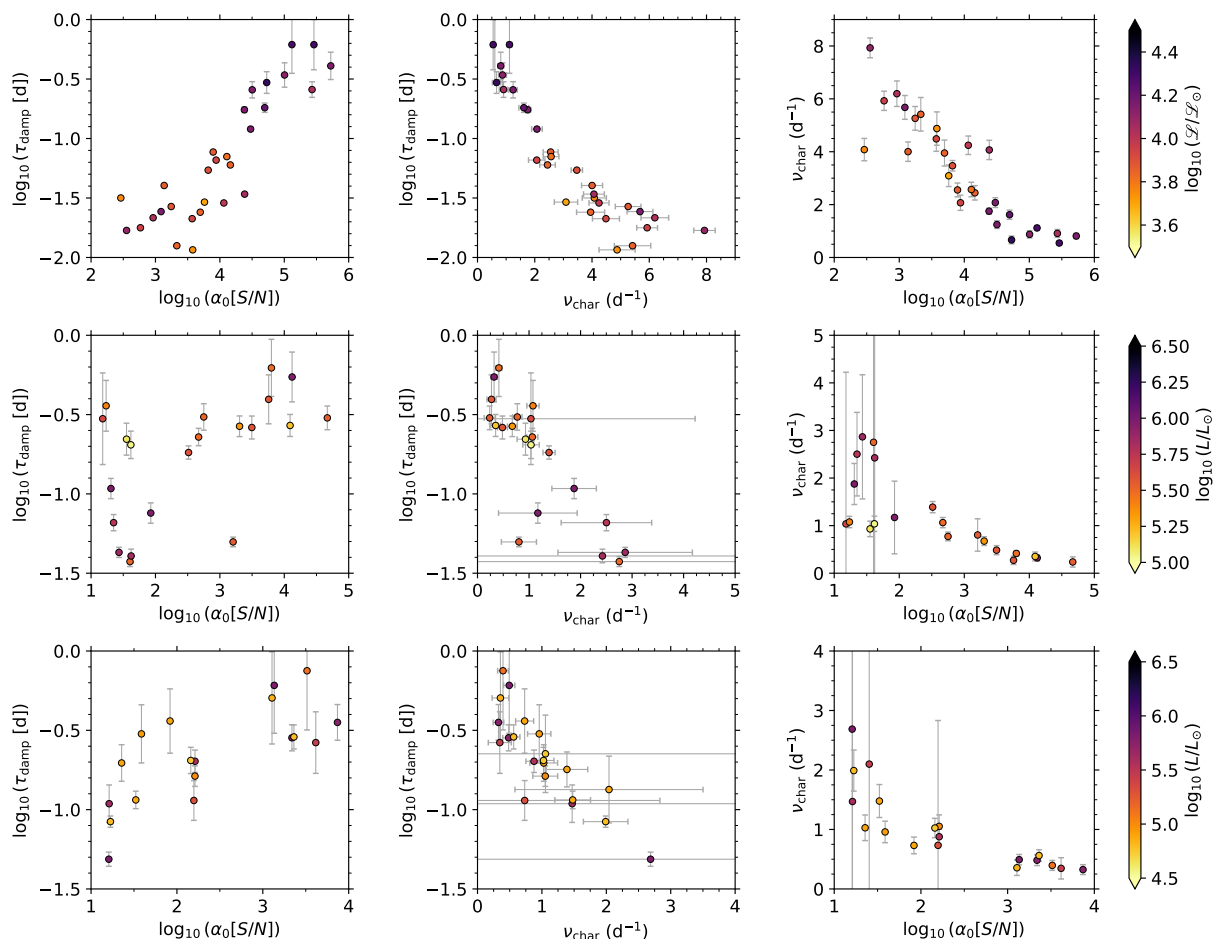


Fig. 3. Correlations between (spectroscopic) luminosity and SLF variability parameters for the sub-samples of Milky Way, LMC, and SMC massive stars studied in this work are shown (from top to bottom). We note that the spectroscopic effective luminosity is defined as $\mathcal{L} := T_{\text{eff}}^4/g$ (Langer & Kudritzki 2014) with values taken from Bowman et al. (2020) for consistency. The uncertainties plotted are the 2σ confidence intervals from the combined methodology of a GP regression and Hamiltonian Monte Carlo with a no U-turn sampler (Bowman & Dorn-Wallenstein 2022).

convection zones, the observed SLF variability could be exclusively caused by IGWs from core convection. Therefore, on balance, these results support the conclusion that 1D structure models cannot be used to rule out core convection as a contributing factor to SLF variability, even if it is arguably not the dominant contributor for Galactic massive stars, which remains to be seen. In addition to metallicity, it is expected from stellar evolution theory and models that sub-surface convection is more important for stars approaching the TAMS given the evolutionary changes to their structures are more conducive to this mechanism than compared to stars near the ZAMS (Bowman 2023).

5. Discussion and conclusions

In this work we demonstrated for the first time that SLF variability is omnipresent in massive stars above $20 M_{\odot}$ in low-metallicity environments when sufficiently high-quality light curves are available. We achieved this using a sub-sample of massive stars in the SMC and LMC galaxies from the XShootU collaboration (Vink et al. 2023). We extracted optimised ePSF light curves from the TESS mission FFI data using the `tg1c` software package (Han & Brandt 2023), and analysed them using a GP regression fitting methodology (Bowman & Dorn-Wallenstein 2022). We find that all SMC massive stars have similar SLF variability morphologies to each other, but also to LMC and Galactic massive stars (Bowman et al. 2019b, 2020;

Bowman & Dorn-Wallenstein 2022). Hence, this demonstrates that the physical mechanism(s) responsible for SLF variability in massive stars appears to be largely independent of a star’s metallicity, and predominantly set by a star’s location in the HR diagram (i.e. a star’s mass and age).

We also find that the morphology of SLF variability in massive stars in the SMC, and in particular its observed amplitude, does not systematically depend on whether a star is within the stability window for sub-surface convection predicted by non-rotating 1D structure models. This is evidenced by SMC massive stars inside and outside of their stability window having similar S/N values in their SLF variability. These stability windows are defined based on the Rayleigh number for convection (Jermyn et al. 2022), and have been updated in this work to include asteroseismically calibrated constraints on interior mixing (Bowman 2020). We note that the approach by Jermyn et al. (2022) to use the Rayleigh number as a definition for the onset of convection produces larger stability windows for SMC stars compared to LMC stars because of their lower metallicities. Owing to the small size of the LMC stability window, it is clear that none of the stars studied in this work fall inside the corresponding sub-surface convection zone stability window even if relatively large confidence intervals for their spectroscopic estimates of effective temperature and luminosity are considered. On the other hand, the fact that the SMC sub-sample includes stars both inside and

outside of the corresponding sub-surface convection zone stability window and have similar SLF variability is a challenge to using 1D structure models for predictions of sub-surface convection as a universal explanation for SLF variability.

Owing to the brightness limit of the TESS mission, our sample with successfully extracted light curves is biased to more massive stars as these are brighter. Moreover, a conclusion on how common SLF variability is between $3 \lesssim M \lesssim 20 M_{\odot}$ in the SMC, as previously claimed for Galactic stars by Bowman et al. (2019a) and Bowman et al. (2019b), cannot be made in this work. The astrophysical bias of our sample is that fainter stars are less massive and if such stars follow the same trend as Galactic stars means they also have smaller amplitude SLF variability, but it is also more difficult to extract light curves for fainter stars. In the future, the ESA PLATO mission (Rauer et al. 2024) will observe the LMC and SMC with smaller pixels, a longer continuous time span, and an improved photometric precision compared to TESS, allowing us to push to fainter stars.

Important limitations of the 1D structure models used in this work and elsewhere in the literature include the lack of rotation, but also uncertainties in opacity tables for stellar interiors (see discussion by Aerts et al. 2018), which may lead to smaller or larger stability windows dependent on how the physical prescriptions for these processes are incorporated in 1D structure models. For example, Jermyn et al. (2022) discuss substantially larger stability windows for rotating 1D structure models, even for very slow rotation periods of 1000 d, and a modest further increase for models with rotation periods between 1000 d and 2 d. However, in all cases studied, as expected, rotation has a stabilising effect for convection because it increases the critical Rayleigh number. This means that our non-rotating stability windows are underestimates of the true size of such regions when realistic rotation rates are considered, which only strengthens our conclusions that convection does not play a role in SLF variability for low-metallicity massive stars.

A full parameter study that allows a range of metallicity values, rotation rates, and chemical mixing processes has not been investigated here and is the subject of future work. For example, rotation breaks the assumption of spherical symmetry and leads to gravity darkening, which would arguably lead to different depths for sub-surface convection as a function of stellar latitude. By extension, this could lead to different SLF variability amplitudes as a function of latitude, meaning one could expect different properties for SLF variability for stars of different inclinations with respect to the observer. Moreover, 1D stellar structure models, including those calculated in this work use mixing-length theory, which has limitations in modelling the true dynamics of convective zones in 3D spherical geometry (see the review by Joyce & Tayar 2023). There is also growing evidence from modern hydrodynamical simulations that convection is extremely inefficient in the sub-surface convection zones of Galactic massive stars and that radiation is the dominant energy transport mechanism (see e.g. Schultz et al. 2022, 2023; Debnath et al. 2024). This begs the question of whether these regions should continue to be called sub-surface convection zones.

A complementary result of this work is that we do not find any convincing cases of massive stars with coherent pulsation modes excited by the heat-engine mechanism in the LMC and SMC targets considered. Studies that combine time series spectroscopy (i.e. identifying spectral line profile variability) with photometry have yielded a lower incidence rate of β Cep and SPB pulsators and a higher incidence rate of pulsating Be stars in the SMC compared to the galaxy (see e.g. Diago et al. 2008). The lower opacities of SMC and LMC massive stars is a natu-

ral explanation for a less efficient heat-engine mechanism exciting coherent pulsation modes (e.g. Salmon et al. 2012). However, predictions of pulsation excitation mechanism based on 1D stellar structure models typically lack rotation and atomic diffusion including radiative levitation, which have both been shown to be important in exciting coherent pulsation modes in Galactic main-sequence B-type stars (Townsend 2005; Szweczek & Daszyńska-Daszkiewicz 2017; Rehm et al. 2024). Interestingly, the reduced incidence of coherent pulsators in the literature and lack of coherent pulsators in our sample further supports the conclusion of weaker (or absent) sub-surface convection zones for low-metallicity stars. Therefore, a natural next step on the theoretical side is to include rotation and atomic diffusion including radiative levitation in the calculations of sub-surface convection zone stability windows for low-metallicity massive stars.

The physical mechanism behind SLF variability in massive stars is debated in the literature, but all currently proposed mechanisms have advantages and limitations when confronted with observations (see the review by Bowman 2023). A much larger sample of SMC massive stars with accurate stellar parameters is expected in the near future and will be highly advantageous to explore the physical mechanisms responsible for SLF variability, which is incorporated within the XShootU (Vink et al. 2023) and BLOeM (Shenar et al. 2024) projects. Regardless, our proof-of-concept study demonstrates that it is possible to probe the excitation mechanism of SLF variability at low metallicity and constrain its dependence on a star's location in the HR diagram. Equally, our results also demonstrate the important limitations of using (non-rotating) 1D structure models for producing observables to be compared to observations of SLF variability.

Finally, our study provides strong motivation for hydrodynamists to perform low-metallicity simulations of massive stars in 3D spherical geometry, and to include realistic rotation rates, since this may elucidate the latitudinal properties of IGWs excited by sub-surface convection and core convection. We postulate that the high diversity in SLF variability morphologies is caused by a combination of unknown inclination angles combined with a wide range of rotational velocities. Thus, a range of latitudinally dependent interior mixing efficiencies may be at work, which are not well calibrated in massive star evolution theory. Specifically, addressing how convection, and also turbulence, generated by a radiation-dominated iron-bump in the envelopes of massive stars produce SLF variability in 3D spherical geometry including rotation is required in order to accurately compare theoretical amplitudes and frequencies of IGWs to observations. In this study the omnipresence of SLF variability across a wide range of metallicity values suggests that convection within the iron bump may play a minor role, especially for younger and lower metallicity massive stars. In the future, a much larger sample of massive stars in the SMC and LMC with accurate spectroscopic parameters delivered by the XShootU and BLOeM projects combined with hydrodynamical simulations will allow a new and exciting dimension to be added to the growing interest in massive star variability studies.

Acknowledgements. The authors thank the referee for useful feedback that improved the clarity of this work, Adam Jermyn for useful discussions and kindly providing well-documented and open-access MESA inlists (https://github.com/adamjermyn/conv_trends) to compute evolution tracks and stability windows, as well as Daniel Leccoanet and Matteo Cantiello for useful discussions during the ‘Probes of Transport in Stars’ workshop hosted at KITP in 2021. This research was supported in part by the National Science Foundation (NSF) under Grant Number NSF PHY-1748958. DMB gratefully acknowledges funding from the Research Foundation Flanders (FWO) by means of a senior postdoctoral fellowship (grant agreement No. 1286521N), an FWO long stay travel grant (agreement No. V411621N), as well as UK Research and Innovation (UKRI) in

the form of a Frontier Research grant under the UK government's ERC Horizon Europe funding guarantee (SYMPHONY; grant number: EP/Y031059/1), and a Royal Society University Research Fellowship (URF; grant number: URF/R1231631). MM gratefully acknowledges funding from FWO by means of a PhD scholarship (11F7120N), and TVR gratefully acknowledges the KU Leuven Research Council (C16/18/005: PARADISE). The authors thank the TESS science team for the excellent data, which were obtained from the Mikulski Archive for Space Telescopes (MAST) at the Space Telescope Science Institute (STScI; <https://archive.stsci.edu/missions-and-data/tess>), which is operated by the Association of Universities for Research in Astronomy, Inc., under NASA contract NAS5-26555. Support to MAST for these data is provided by the NASA Office of Space Science via grant NAG5-7584 and by other grants and contracts. Funding for the TESS mission is provided by the NASA Explorer Program. This research has made use of the SIMBAD database, operated at CDS, Strasbourg, France; the SAO/NASA Astrophysics Data System; and the VizieR catalog access tool, CDS, Strasbourg, France. This research has made use of the following software packages: `tg1c` (Han & Brandt 2023) for light curve extraction (https://github.com/TeHanHunter/TESS_Gaia_Light_Curve), `celerite2` (Foreman-Mackey et al. 2017) for GP regression fitting (<https://celerite2.readthedocs.io/en/latest/>) and `pymc3` (Salvatier et al. 2016) for confidence interval estimation (<https://github.com/pymc-devs/pymc>), as well as `matplotlib` (Hunter 2007), `seaborn` (Waskom 2021), and `numpy` (Oliphant 2006; van der Walt et al. 2011; Harris et al. 2020). For the purpose of open access, the authors have applied a CC BY licence to the author accepted manuscript version: <https://arxiv.org/abs/2410.12726>. Data products that support the results in this paper are publicly available via the Zenodo repository: <https://zenodo.org/records/14018449>.

References

- Aerts, C. 2021, *Reviews of Modern Physics*, 93, 015001
- Aerts, C., Christensen-Dalsgaard, J., & Kurtz, D. W. 2010, *Asteroseismology* (Springer)
- Aerts, C., Molenberghs, G., Michielsen, M., et al. 2018, *ApJS*, 237, 15
- Aerts, C. & Rogers, T. M. 2015, *ApJ*, 806, L33
- Aerts, C., Thoul, A., Daszyńska, J., et al. 2003, *Science*, 300, 1926
- Anders, E. H., Lecoanet, D., Cantiello, M., et al. 2023, *Nature Astronomy*, 7, 1228
- Auvergne, M., Bodin, P., Boisnard, L., et al. 2009, *A&A*, 506, 411
- Blomme, R., Mahy, L., Catala, C., et al. 2011, *A&A*, 533, A4
- Borucki, W. J., Koch, D., Basri, G., et al. 2010, *Science*, 327, 977
- Bouret, J. C., Lanz, T., Martins, F., et al. 2013, *A&A*, 555, A1
- Bowman, D. M. 2020, *Frontiers in Astronomy and Space Sciences*, 7, 70
- Bowman, D. M. 2023, *Ap&SS*, 368, 107
- Bowman, D. M., Aerts, C., Johnston, C., et al. 2019a, *A&A*, 621, A135
- Bowman, D. M., Burssens, S., Pedersen, M. G., et al. 2019b, *Nature Astronomy*, 3, 760
- Bowman, D. M., Burssens, S., Simón-Díaz, S., et al. 2020, *A&A*, 640, A36
- Bowman, D. M. & Dorn-Wallenstein, T. Z. 2022, *A&A*, 668, A134
- Bowman, D. M., Vandenbussche, B., Sana, H., et al. 2022, *A&A*, 658, A96
- Bradley, L., Sipőcz, B., Robitaille, T., et al. 2022, *astropy/photutils: 1.5.0*
- Briquet, M., Aerts, C., Baglin, A., et al. 2011, *A&A*, 527, A112
- Briquet, M., Neiner, C., Aerts, C., et al. 2012, *MNRAS*, 427, 483
- Burssens, S., Bowman, D. M., Michielsen, M., et al. 2023, *Nature Astronomy*, 7, 913
- Burssens, S., Simón-Díaz, S., Bowman, D. M., et al. 2020, *A&A*, 639, A81
- Cantiello, M., Langer, N., Brott, I., et al. 2009, *A&A*, 499, 279
- Cantiello, M., Lecoanet, D., Jermyn, A. S., & Grassitelli, L. 2021, *ApJ*, 915, 112
- Debnath, D., Sundqvist, J. O., Moens, N., et al. 2024, *A&A*, 684, A177
- Degroote, P., Aerts, C., Ollivier, M., et al. 2009, *A&A*, 506, 471
- Diago, P. D., Gutiérrez-Soto, J., Fabregat, J., & Martayan, C. 2008, *A&A*, 480, 179
- Dupret, M.-A., Thoul, A., Scuflaire, R., et al. 2004, *A&A*, 415, 251
- Dziembowski, W. A., Moskalik, P., & Pamyatnykh, A. A. 1993, *MNRAS*, 265, 588
- Dziembowski, W. A. & Pamyatnykh, A. A. 1993, *MNRAS*, 262, 204
- Dziembowski, W. A. & Pamyatnykh, A. A. 2008, *MNRAS*, 385, 2061
- Edelmann, P. V. F., Ratnasingham, R. P., Pedersen, M. G., et al. 2019, *ApJ*, 876, 4
- Foreman-Mackey, D., Agol, E., Ambikasaran, S., & Angus, R. 2017, *AJ*, 154, 220
- Foreman-Mackey, D., Agol, E., Angus, R., et al. 2019, *dfm/celerite: celerite v0.3.1*
- Gaia Collaboration, Prusti, T., de Bruijne, J. H. J., et al. 2016, *A&A*, 595, A1
- Gaia Collaboration, Vallenari, A., Brown, A. G. A., et al. 2023, *A&A*, 674, A1
- Han, T. & Brandt, T. D. 2023, *AJ*, 165, 71
- Harris, C. R., Millman, K. J., van der Walt, S. J., et al. 2020, *Nature*, 585, 357
- Hawcroft, C., Sana, H., Mahy, L., et al. 2024, *A&A*, 688, A105
- Herwig, F., Woodward, P. R., Mao, H., et al. 2023, *MNRAS*, 525, 1601
- Horst, L., Edelmann, P. V. F., Andrásy, R., et al. 2020, *A&A*, 641, A18
- Howell, S. B., Sobeck, C., Haas, M., et al. 2014, *PASP*, 126, 398
- Hunter, I., Brott, I., Lennon, D. J., et al. 2008, *ApJ*, 676, L29
- Hunter, J. D. 2007, *Computing in Science and Engineering*, 9, 90
- Jenkins, J. M., Twicken, J. D., McCauliff, S., et al. 2016, in *Proc. SPIE*, Vol. 9913, *Software and Cyberinfrastructure for Astronomy IV*, 99133E
- Jermyn, A. S., Anders, E. H., & Cantiello, M. 2022, *ApJ*, 926, 221
- Jermyn, A. S., Bauer, E. B., Schwab, J., et al. 2023, *ApJS*, 265, 15
- Joyce, M. & Tayar, J. 2023, *Galaxies*, 11, 75
- Koch, D. G., Borucki, W. J., Basri, G., et al. 2010, *ApJ*, 713, L79
- Krtićka, J. & Feldmeier, A. 2018, *A&A*, 617, A121
- Krtićka, J. & Feldmeier, A. 2021, *A&A*, 648, A79
- Langer, N. & Kudritzki, R. P. 2014, *A&A*, 564, A52
- Le Saux, A., Baraffe, I., Guillet, T., et al. 2023, *MNRAS*, 522, 2835
- Lecoanet, D., Bowman, D. M., & Van Reeth, T. 2022, *MNRAS*, 512, L16
- Lecoanet, D., Cantiello, M., Anders, E. H., et al. 2021, *MNRAS*, 508, 132
- Lecoanet, D., Cantiello, M., Quataert, E., et al. 2019, *ApJ*, 886, L15
- Michielsen, M., Aerts, C., & Bowman, D. M. 2021, *A&A*, 650, A175
- Miglio, A., Montalbán, J., & Dupret, M.-A. 2007, *MNRAS*, 375, L21
- Mokiem, M. R., de Koter, A., Evans, C. J., et al. 2007, *A&A*, 465, 1003
- Mokiem, M. R., de Koter, A., Evans, C. J., et al. 2006, *A&A*, 456, 1131
- Oliphant, T. E. 2006, *A guide to NumPy*, Vol. 1 (Trelgol Publishing USA)
- Pamyatnykh, A. A., Handler, G., & Dziembowski, W. A. 2004, *MNRAS*, 350, 1022
- Paxton, B., Bildsten, L., Dotter, A., et al. 2011, *ApJS*, 192, 3
- Paxton, B., Cantiello, M., Arras, P., et al. 2013, *ApJS*, 208, 4
- Paxton, B., Marchant, P., Schwab, J., et al. 2015, *ApJS*, 220, 15
- Paxton, B., Schwab, J., Bauer, E. B., et al. 2018, *ApJS*, 234, 34
- Paxton, B., Smolec, R., Schwab, J., et al. 2019, *ApJS*, 243, 10
- Pedersen, M. G., Aerts, C., Pápics, P. I., et al. 2021, *Nature Astronomy*, 5, 715
- Ramírez-Agudelo, O. H., Simón-Díaz, S., Sana, H., et al. 2013, *A&A*, 560, A29
- Ratnasingham, R. P., Edelmann, P. V. F., & Rogers, T. M. 2019, *MNRAS*, 482, 5500
- Ratnasingham, R. P., Edelmann, P. V. F., & Rogers, T. M. 2020, *MNRAS*, 497, 4231
- Ratnasingham, R. P., Rogers, T. M., Chowdhury, S., et al. 2023, *A&A*, 674, A134
- Rauer, H., Aerts, C., Cabrera, J., et al. 2024, arXiv e-prints, arXiv:2406.05447
- Rehm, R., Mombarg, J. S. G., Aerts, C., et al. 2024, *A&A*, 687, A175
- Ricker, G. R., Winn, J. N., Vanderspek, R., et al. 2015, *Journal of Astronomical Telescopes, Instruments, and Systems*, 1, 014003
- Rogers, T. M. 2015, *ApJ*, 815, L30
- Rogers, T. M., Lin, D. N. C., McElwaine, J. N., & Lau, H. H. B. 2013, *ApJ*, 772, 21
- Roman-Duval, J., Proffitt, C. R., Taylor, J. M., et al. 2020, *Research Notes of the American Astronomical Society*, 4, 205
- Salmon, S., Montalbán, J., Morel, T., et al. 2012, *MNRAS*, 422, 3460
- Salmon, S. J. A. J., Moyano, F. D., Eggenberger, P., Haemmerlé, L., & Buldgen, G. 2022, *A&A*, 664, L1
- Salvatier, J., Wiecki, T. V., & Fonnesbeck, C. 2016, *PyMC3: Python probabilistic programming framework*
- Sana, H., de Mink, S. E., de Koter, A., et al. 2012, *Science*, 337, 444
- Schultz, W. C., Bildsten, L., & Jiang, Y.-F. 2022, *ApJ*, 924, L11
- Schultz, W. C., Bildsten, L., & Jiang, Y.-F. 2023, *ApJ*, 951, L42
- Shenar, T., Bodensteiner, J., Sana, H., et al. 2024, *A&A*, 690, A289
- Szewczuk, W. & Daszyńska-Daszkiewicz, J. 2017, *MNRAS*, 469, 13
- Thompson, W., Herwig, F., Woodward, P. R., et al. 2024, *MNRAS*, 531, 1316
- Townsend, R. H. D. 2005, *MNRAS*, 364, 573
- Van Daele, P. 2023, Master's thesis, KU Leuven, Belgium
- van der Walt, S., Colbert, S. C., & Varoquaux, G. 2011, *Computing in Science Engineering*, 13, 22
- Vanon, R., Edelmann, P. V. F., Ratnasingham, R. P., Varghese, A., & Rogers, T. M. 2023, *ApJ*, 954, 171
- Varghese, A., Ratnasingham, R. P., Vanon, R., Edelmann, P. V. F., & Rogers, T. M. 2023, *ApJ*, 942, 53
- Vernet, J., Dekker, H., D'Odorico, S., et al. 2011, *A&A*, 536, A105
- Vink, J. S., Mehner, A., Crowther, P. A., et al. 2023, *A&A*, 675, A154
- Waskom, M. L. 2021, *Journal of Open Source Software*, 6, 3021
- Weiss, W. W., Rucinski, S. M., Moffat, A. F. J., et al. 2014, *PASP*, 126, 573
- Weiss, W. W., Zwintz, K., Kuschnig, R., et al. 2021, *Universe*, 7, 199
- Zwintz, K., Pigulski, A., Kuschnig, R., et al. 2024, *A&A*, 683, A49

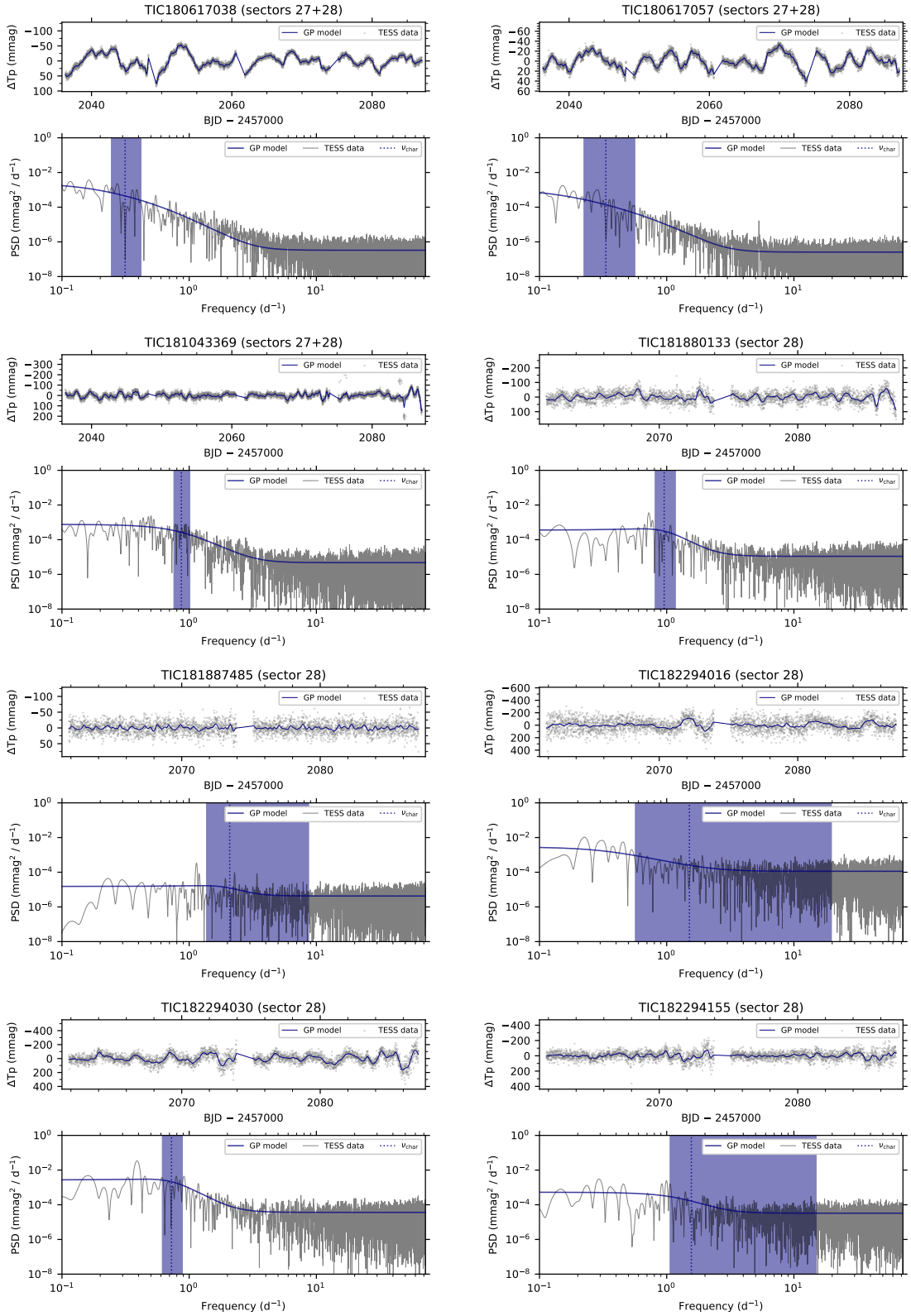


Fig. A.1. Extracted ePSF light curves using `tg1c` (Han & Brandt 2023) and fitted with the GP regression methodology of Bowman & Dorn-Wallenstein (2022) for SMC massive stars.

Appendix A: Additional figures

The extracted ePSF light curves using the `tg1c` software package (Han & Brandt 2023) fitted with the GP regression methodology of Bowman & Dorn-Wallenstein (2022) for SMC and LMC massive stars are shown in Figs. A.1–A.3 and Figs. A.4–A.6, respectively.

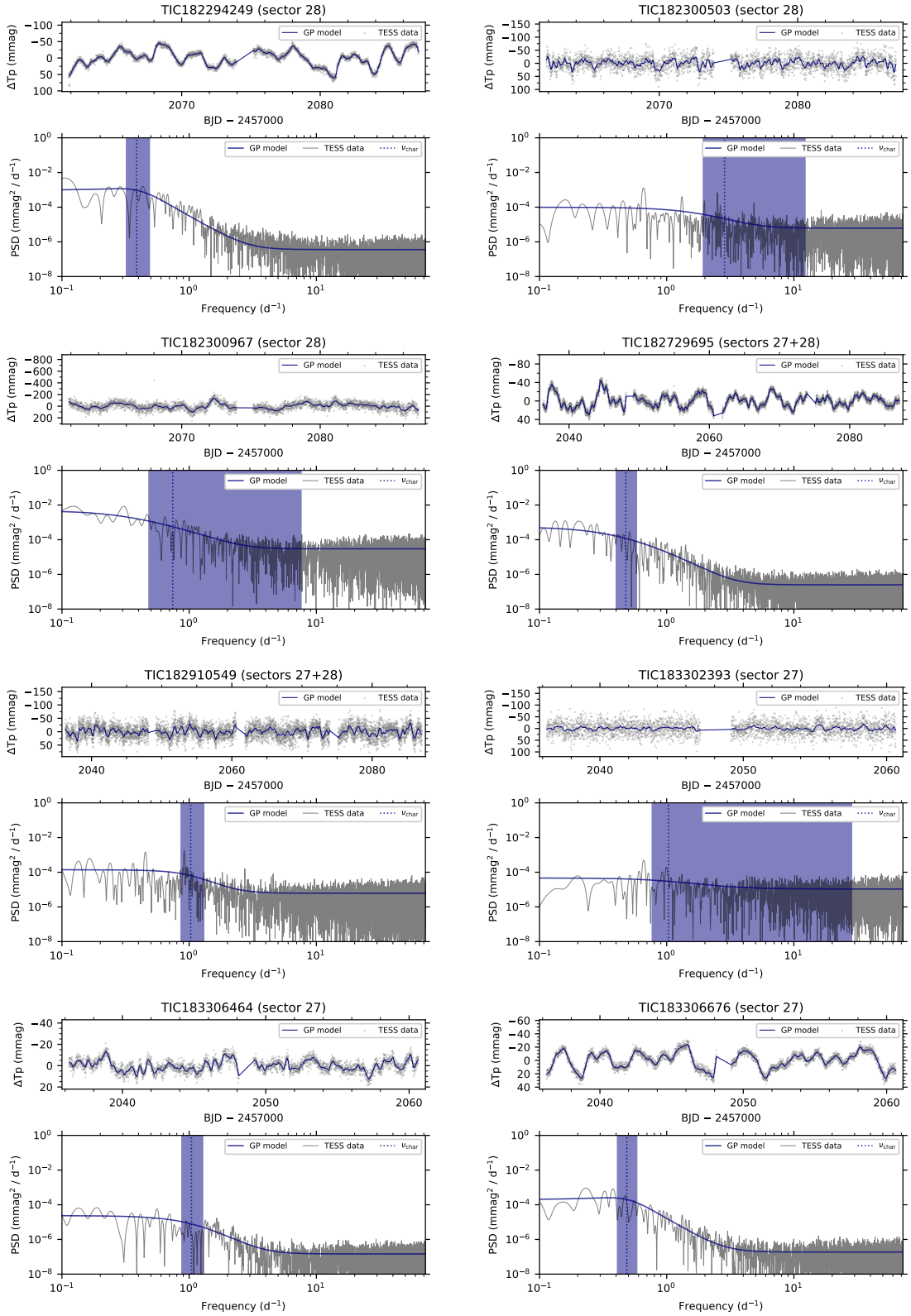


Fig. A.2. Extracted ePSF light curves using `tg1c` (Han & Brandt 2023) and fitted with the GP regression methodology of Bowman & Dorn-Wallenstein (2022) for SMC massive stars (*continued*).

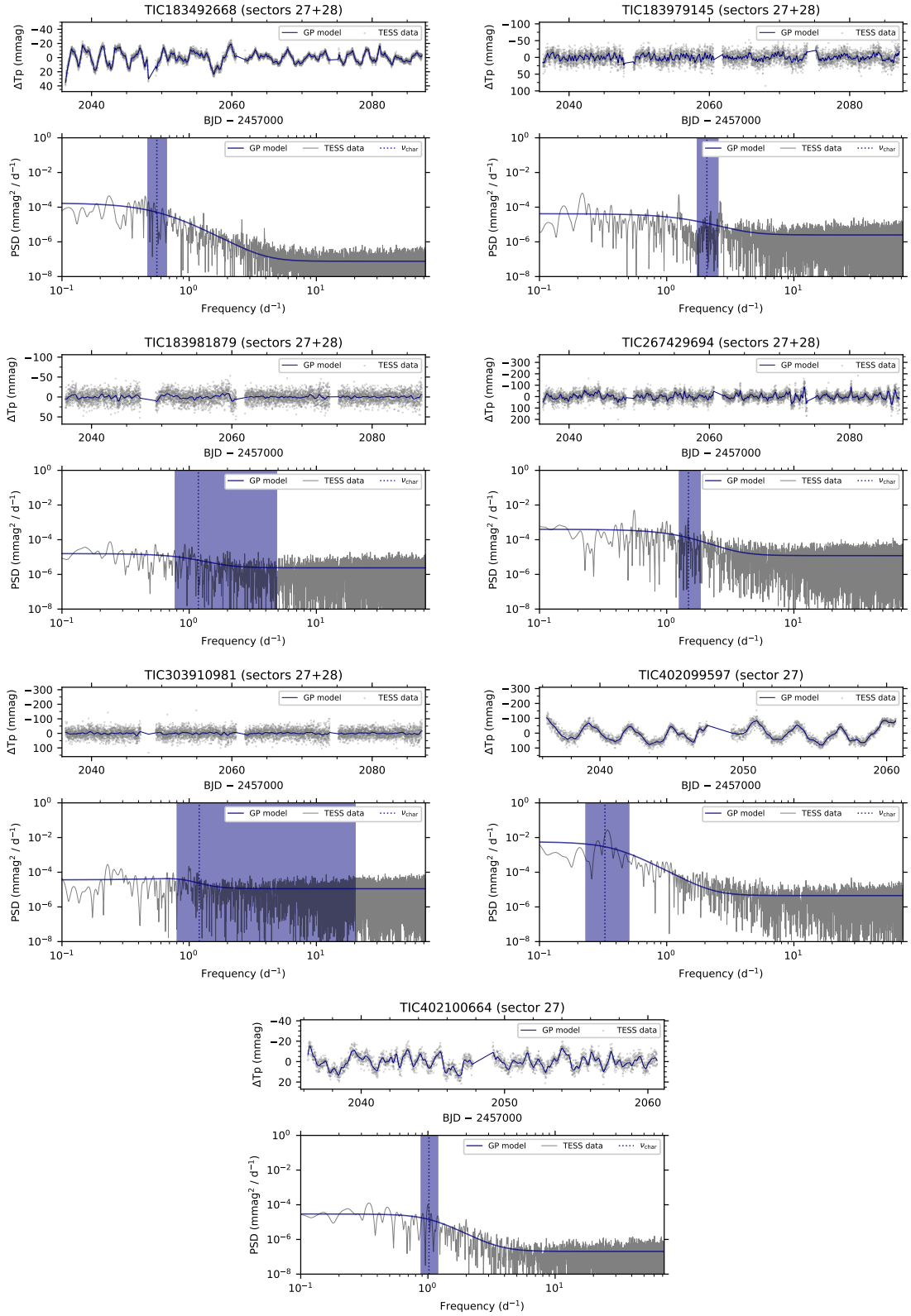


Fig. A.3. Extracted ePSF light curves using `tg1c` (Han & Brandt 2023) and fitted with the GP regression methodology of Bowman & Dorn-Wallenstein (2022) for SMC massive stars (*continued*).

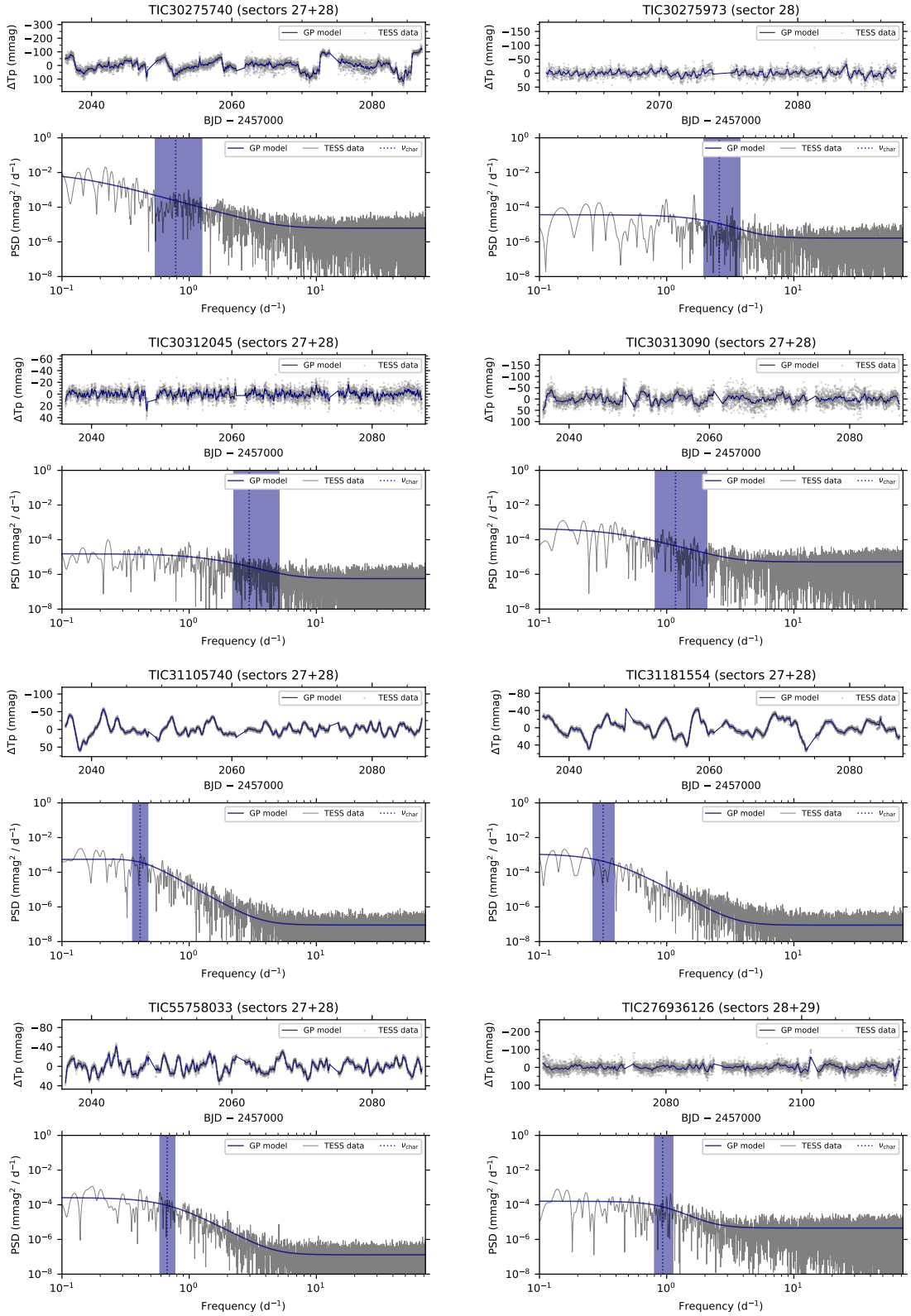


Fig. A.4. Extracted ePSF light curves using `tg1c` (Han & Brandt 2023) and fitted with the GP regression methodology of Bowman & Dorn-Wallenstein (2022) for LMC massive stars.

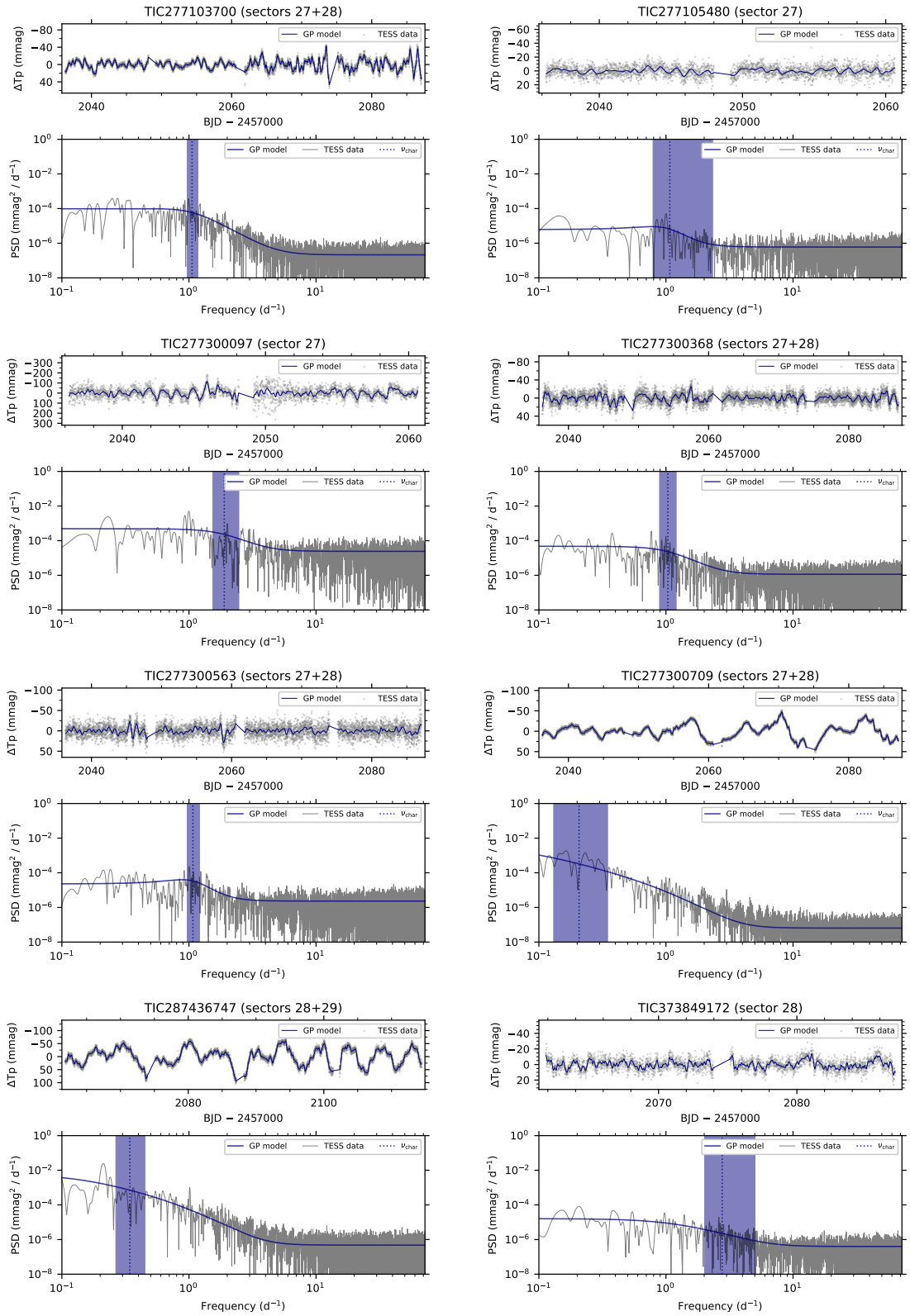


Fig. A.5. Extracted ePSF light curves using `tg1c` (Han & Brandt 2023) and fitted with the GP regression methodology of Bowman & Dorn-Wallenstein (2022) for LMC massive stars (*continued*).

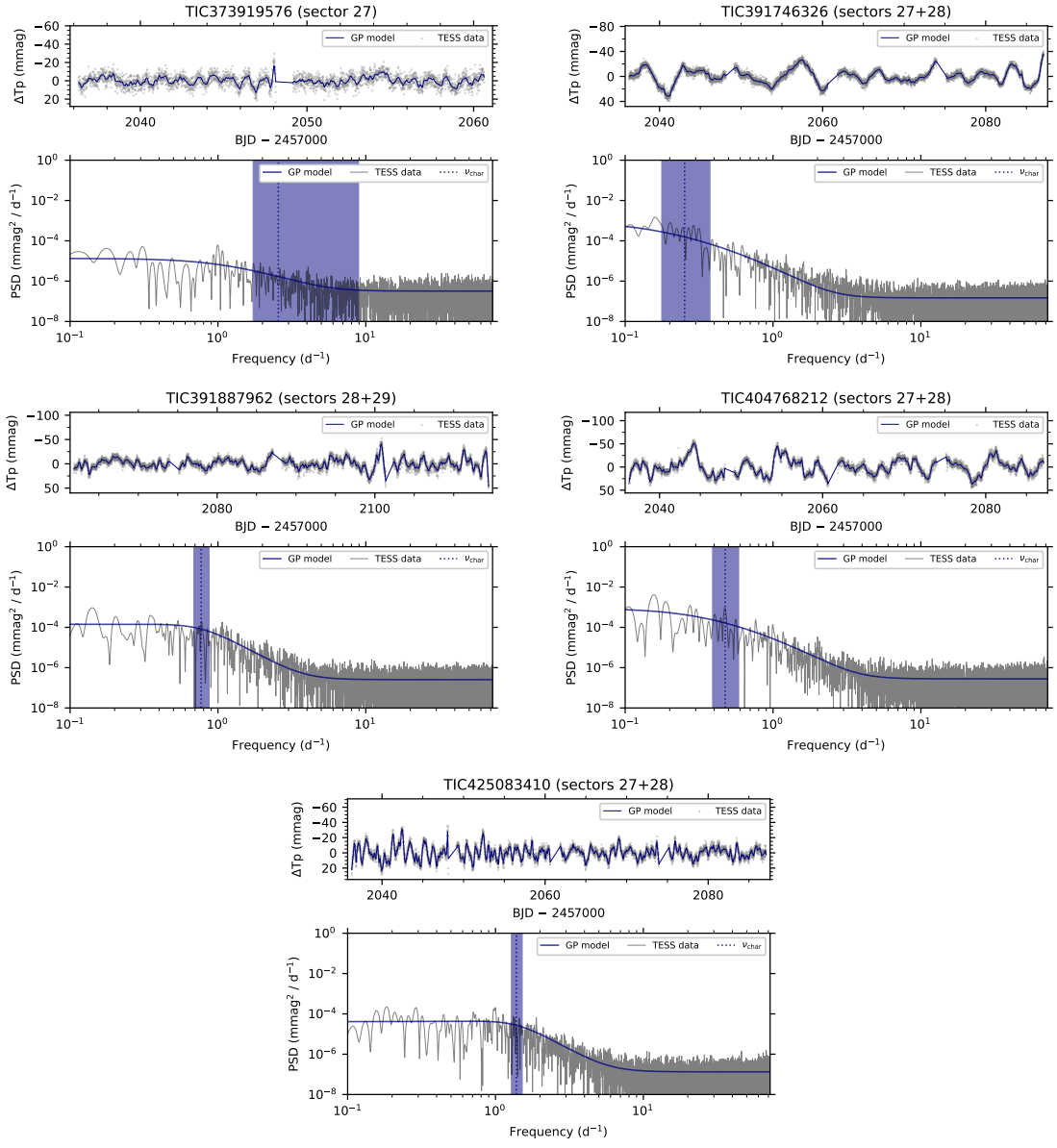


Fig. A.6. Extracted ePSF light curves using `tg1c` (Han & Brandt 2023) and fitted with the GP regression methodology of Bowman & Dorn-Wallenstein (2022) for LMC massive stars (*continued*).